Rev. Adv. Mater. Sci. 51 (2017) 160-176

NANOTWINNED COPPER-GRAPHENE FOILS – A BRIEF REVIEW

V.G. Konakov[1,2], O.Yu. Kurapova[1,2], A.S. Grashchenko[3], S.N. Golubev[4], E.N. Solovyeva[2,4] and I.Yu. Archakov[1,3]

[1]Peter the Great St. Petersburg Polytechnic University, St. Petersburg 195251, Russia
[2]St. Petersburg State University, St. Petersburg, 199034, Russia
[3]Institute for Problems of Mechanical Engineering, Russian Academy of Sciences, St. Petersburg, 199178, Russia
[4]Glass and Ceramics Ltd., St. Petersburg, 199004, Russia

Received: May 28, 2017

Abstract. The paper reviews the approaches for copper-graphene composites synthesis. The optimization of electrochemical deposition method both for pure nanotwinned copper and nanotwinned copper - graphene foils production is discussed. It is shown that two-step deposition including the buffer pure nanotwinned copper layer deposition followed by copper-graphene layer deposition provides the nanotwinned modification of the metal in the material matrix. The analysis of the effect of non-ionic surfactants used to stabilize graphene concentration in sulfur electrolyte during the long-time deposition gives an opportunity to consider surfactants application as a promising approach to solve this task. Summary of the mechanical test results shows the positive effect of graphene introduction on the mechanical properties of the material.

1. INTRODUCTION

Nowadays, nanotwinned metals are considered as very perspective type of materials for various applications in modern industry. One of their doubtless advantages is the possibility of the significant improvement in the mechanical properties of nanotwinned metals in comparison with having ordered microstructure (coarse and fine grained), see the review by I.A. Ovid'ko and A.G. Sheinerman [1]. In particular, such properties as hardness (including microhardness), strength, and crack resistance can be significantly improved, see the examples in [2-4].

The use of nanotwinned copper is fairly important. Despite the fact that Cu possesses quite high electro- and heat conductivities, it suffers from rather low mechanical properties. Some works performed in this field demonstrated the possibility to improve these characteristics due to the use of nanotwinned copper. Let us consider these achievements in more detail. First, the pioneer works of Lei Lu with coauthors, see, e.g. [5-8], proving the outstanding properties of electrodeposited nanotwinned copper should be mentioned.

Paper [5] analyzes the comparison of the true stress values obtained for nanotwinned (NT), nanocrystalline (NC), and coarse-grained (CG) copper. It is demonstrated that the true stress determined for NT Cu 3-5 times exceeds the values shown for CG one. It is stated that the data on true stress of NC copper are limited by a rather narrow true strain range (less than 1.5%, while the data for NT and CG copper are given for 0-15% range), however, the approximation of the stress-strain curve for a wider range gives an opportunity to claim that the true stress of NT copper is also higher than that

Corresponding author: V.G. Konakov, e-mail: glasscer@yandex.ru

for NC Cu. It could be expected that the use of the nanotwinned copper modification can produce twice increase in the true strain of the material as compared to NC Cu. The resulted increase in mechanical properties did not affect such an important copper characteristic as electroconductivity. Indeed, the resistivity of NT Cu is quite comparable with that of CG copper, while the resistivity of NC copper is much higher. Paper [6], compares the variation in the yield strength and strain hardening coefficient obtained for NT and NC copper. Analyzing the data presented in [6] one could conclude that the yield strength values for NT and NC Cu are quite close; however, it is stated that the curve for NT copper is characterized by the presence of maximum of 900 MPa at twin thickness of ~ 15 nm. It is also mentioned that the strain hardening coefficient of NT Cu in the nanosized region (twin thickness/grain sizes lower than 100 nm) is much higher than that of NC copper, while the opposite behavior is observed at higher typical linear dimensions. The suggestions on the strain mechanisms governing the strain hardening in NT copper are presented. In particular, the competition between dislocation-dislocation interaction hardening in coarse twins and twin boundary-dislocation interaction in fine twins are considered. Paper [7] reports the effect of the cold rolling (at room and liquid nitrogen temperatures, RT and LNT, respectively) on the microhardness of NT copper. It is shown that rolling at LNT could increase the microhardness of nanotwinned copper as compared with the results obtained at RT. Moreover, the increase in the rolling strain up to 40% at LNT resulted in 15-20% increase in microhardness, in contrast, similar increase at RT gave rise to 3-5% decrease in microhardness. Considering the deformation mechanisms, the authors attributed the above discussed behavior to the changes in the nanotwinned state of the material. Paper [8] discusses the tensile behavior of nanotwinned Cu and its microstructure.

The pioneer works of L. Lu were followed by a number of papers, most of the proved them unique characteristics of nanotwinned copper, e.g. [9,10]. You et al. [9] analyzed deformation mechanisms in the nanotwinned metals, NT stress-strain dependencies and its microhardness were discussed in detail. Choi et al. [10] described the peculiarities of the nanoindentation test application for the case of nanotwinned copper.

Summarizing the above information, we can state that nanotwinning significantly increases the copper mechanical properties. However, some extra increase could be expected due to graphene (Gr) reinforcement of the material. Indeed, graphene as a form of carbon possesses the values of heat and electroconductivity close to that of copper. So, the introduction of graphene in the copper foil matrix should not decrease the material electrical and heat transfer characteristics. On the other hand, the excellent mechanical features of graphene are well known (e.g., C. Lee [11] estimated the graphene hardness as ~ 130 GPa, while its Yang modulus was ~ 1 TPa). The positive effect of Gr reinforcement on the mechanical properties of metal-graphene composites was reported many times, see, e.g. [12,13]. These positive results are very promising due to the fact that previous attempts to improve copper properties by oxide/carbide nanoparticles introduction [14-17], as well as approaches based on by carbon nanotubes and nanowires addition [18-21] faced serious problems. It can be concluded that reinforcement by oxide/carbide nanoparticles increases the mechanical properties of copper-based composites; regretfully, the values of electro- and heat conductivities in such materials are usually lower than those of pure copper. Carbon nanomaterials like nanowires and nanotubes provide quite a positive effect: the mechanical properties of such composites were improved at stable characteristics of electro- and heat conductivities. The general problem here was the material microstructure. Due to the relatively extended linear dimensions of the carbon additives and their tendency to agglomerate, final material was characterized by rather high porosity and non-uniform microstructure. So, the use of graphene with its flat geometry [22] resulting in the absence of pores in the final material could be considered as an optimal problem solution.

Let us consider some results in this field in more detail. K. Jagannadham [22] reported composite Cu-Gr foils manufactured by electrochemical deposition at direct current (DC). It was shown that, similarly to the case of carbon nanotubes and nanowires introduction, the high electrical and heat transfer properties are typical for Cu-Gr foil ($2\ 10^{-6}$ Ohm*cm and 460 W/m*K). The attempts to produce Cu-Gr composite consisting of altering copper and graphene monolayers with the layer thickness of 70 nm were performed by Y. Kim et al., see [24]. Gr reinforcement here resulted in the increased hardness and strength, however, the plasticity and elasticity of the material decreased due to the specific structure of the material consisting of different materials layers. Authors of [25,26] showed that NT structure provides the required ratio between hardness and elasticity of the material. Cu-Gr foils with

improved hardness (~2.5 GPa) coupled with rather high elasticity modulus (137 GPa) were reported by C.L. Pavithra et al., [27]. These foils were deposited using alternating current (AC) regime for electrochemical deposition, split graphene oxide was used as a graphene source here. It should be mentioned that, similarly to [22], graphene reinforcement here did not impair electrical and heat transfer properties of the material.

Electrochemical deposition was shown to be cheap and rather simple approach both for NT Cu and metal-Gr foils production (see [5-9,27,28]. However, some principle problems exist here. First one is the necessity to achieve homogeneous graphene containing suspension in $CuSO_4$ electrolyte, which could be stable during the deposition process. Long-time deposition process causes suspension destabilization and graphene sedimentation. A number of approaches targeted on the elimination of Gr sedimentation were suggested in [29-31]. The use of chemical vapor deposition (CVD) or molecular beam epitaxy (MBE) techniques instead of electrochemical deposition results in high cost of the product and very complex equipment/procedure. The general solution suggested by many authors is a mixing of the graphene containing electrolyte before the deposition onset via ultrasound or/and inert gas flow. Such an approach provides the uniform graphene distribution in the electrolyte; however, the stability of graphene containing suspension is limited by short-time period only. Ultrasound treatment applied directly during the deposition process can be probably implied, however, it leads to rapid increase of the electrolyte temperature. Thus, extra cooling would be necessary.

The other problem is to support the required structural reorientation i.e. the percentage of nanotwinned crystals. As it was shown in the works of L. Lu, NT Cu formation requires rather strict deposition conditions. The presence of graphene in the electrolyte leads to the appearance of the additional growth centers (nuclei) on the cathode surface that necessarily reorients the structure of the growing layers. Hence, the task of NT copper-graphene foil production is even more difficult than pure NT copper film growth.

Summarizing this Section, we can state that NT Cu-Gr foils are the perspective materials for a wide range of industry application. The approach to produce pure NT copper layers suggested by L. Lu et al is based on electrochemical deposition; the obtained results demonstrate the possibility to produce high quality NT copper foils with improved mechanical properties and good electro- and heat conductivity. Some attempts to produce NT Cu-Gr foils faced two basic problems: (i) the necessity to support the constant graphene content in the electrolyte during the long-time deposition and (ii) the need to save the nanotwinned mode of the metal matrix in the presence of the additional growth centers. A study to solve these problems was initiated by Prof. Ilya A. Ovid'ko in 2014; the present paper reviews the results of this work.

2. PURE NANOTWINNED COPPER

2.1. Deposition procedures

Inspired by works of L. Lu et al., we have used the electrochemical approach for the tasks of composite NTCu-Gr foils manufacturing, see our paper [32]. The following experimental setup was used. Copper sulfate ($CuSO_4$) ethanol-aqueous and pure aqueous solutions were used as electrolytes. Electrochemical deposition cell consisting of two electrodes with an anode made from pure copper (>99.99 at.%) and cathode manufactured from stainless steel (X10CrNi18-8, i.e. SAE grade 301) was used. AC and DC (altering and direxct current, respectively) deposition regimes were tested.

Generally, the procedure of the electrolyte preparation was as following. Copper sulfate hydrate $CuSO_4*6H_2O$ (99.99%) was dissolved in a distilled water at room temperature up to 1 M concentration and the required amount of ethanol was added; after that, the solution was acidified up to pH=1 by the sulfuric acid. Solutions NN 1,2, and 3 differed in the ethanol content, it was 0, 75, and 37.5 mL/L, respectively.

A number of cell geometries were tested. In the first one (Cell #1), the anode was performed as a copper rod, it was placed into the ∅ 60 mm glass cylinder. The cathode (stainless steel foil) was adjusted to the cylinder walls. Following [5], 1/30 anode-to-cathode surface ratio was chosen, DC of 0.5 A was applied for 1 hour. Solutions NN 1-3 were used to produce Samples 1-3, respectively. Coplanar electrodes (25x20x5 mm stainless steel cathode and 100x80x5 mm copper anode with 30 mm distance between them) were used in Cell#2 design. Note that the anode-to-cathode surface ratio here was inverted and anode surface 16 times exceeded the cathode surface. The same deposition conditions were used in Cell 2, Sample 4 was deposited from Solution N3. Cell#3 geometry was quite similar to that in case of Cell#2, the basic difference here was in the deposition regime. Pulse current regime (pulse on-time of 0.02 s, off-time 2 s) was used here. Since the layers growth rate at elevated

Table 1. List of deposition procedures for NT Cu samples ##1-5.

Sample	Electrolyte	Cell geometry	Deposition conditions
1	Solution N1, 1 M $CuSO_4$*$6H_2O$, acidified by H_2SO_4 up to pH=1	Cell #1∅ 60 mm glass cylinder, 1/30 anode-to cathode ratio	DC 0.5 A for 1 hour
2	Solution N2, 1 M $CuSO_4$*$6H_2O$, acidified by H_2SO_4 up to pH=1,	Cell #1∅ 60 mm glass cylinder, 1/30 anode-to cathode ratio	DC 0.5 A for 1 hour
3	ethanol content 75 mL/L Solution N3, 1 M $CuSO_4$*$6H_2O$, acidified by H_2SO_4 up to pH=1, ethanol content 37.5 mL/L	Cell #1∅ 60 mm glass cylinder, 1/30 anode-to cathode ratio	DC 0.5 A for 1 hour
4	Solution N3, 1 M $CuSO_4$*$6H_2O$, acidified by H_2SO_4 up to pH=1, ethanol content 37.5 mL/L	Cell #2Coplanar electrodes (25x20x5 mm stainless steel cathode and 100x80x5 mm copper anode with 30 mm distance between them)	DC 0.5 A for 1 hour
5	Solution N3, 1 M $CuSO_4$*$6H_2O$, acidified by H_2SO_4 up to pH=1, ethanol content 37.5 mL/L	Cell #3Coplanar electrodes (25x20x5 mm stainless steel cathode and 100x80x5 mm copper anode with 30 mm distance between them)	Pulse regime (0.02 s on-time, 2 s off-time, 02 mA for 24 hours)

carrent values was too high for twins formation, the effective peak current was decreased to 0.2 mA, and, in order to manufacture films with comparable to DC experiments thickness, the deposition time was increased up to 24 hours. Sample 5 was manufactured under these conditions.

All Samples produced were washed in the distilled water, dried by ethanol, and then copper foil was partly removed from the stainless steel substrate. However, the thickness of Sample 5 in spite of long-time deposition was not enough to remove it from the cathode. Table 1 summarized the above production regimes for Samples 1-5.

2.2. Testing approaches and equipment

A convenient set of experimental approaches was used to characterize the samples produced. X-ray diffraction (XRD, Shimadzu XRD-6000, Cu K_a with λ = 1.54 Å, analysis room temperature) was performed to identify phase composition. Samples microstructure was characterized by the scanning electron microscopy (SEM, Zeiss Supra V-55); both outer and internal (adjacent to cathode) surfaces were examined. Electron back scattering diffraction (EBSD, TESCAN MIRA 3LMH FEG scanning electron microscope equipped with an EBSD analyzer "CHANNEL 5",rectangular grid with scan step of 50 nm, standard clean-up procedures involving a grain tolerance angle of 5° and a minimum grain size of three pixels) was used to prove the twinned copper modification and to estimate the grain size in the grown film. Nanoindentation tests were carried out using NanoTest (Micro Materials Co.) equipment.

2.3. Discussion of the experimental results

Regretfully, the application of pulse regime (Sample 5) could not be considered as successful since the growth rate of the film was quite low. The final film thickness after 24-hour deposition was rather low and it was impossible to separate this film from the cathode surface. Despite the fact that growth rates provided by DC deposition regime were relatively high (more than 250 mm per hour), NT copper crystals have formed sucessfully. Hence, the use of pulse regime was considered impractical, the Section below discusses the results obtained for Samples 1-4 produced in DC regime.

Phase composition of all Samples was identified by XRD. It was shown that XRD patterns for all samples were quite similar, the same reflexes with the same ratio were detected for all samples. Fig. 1 demonstrates such patterns detected for inner and outer surfaces of Sample 4. The following conclusions could be done from the analysis of the XRD data. First, copper is the only phase of the grown film, no contaminations are observed in the limit of XRD sensitivity, this statement was later proved by EDX data that is more sensitive approach. Second,

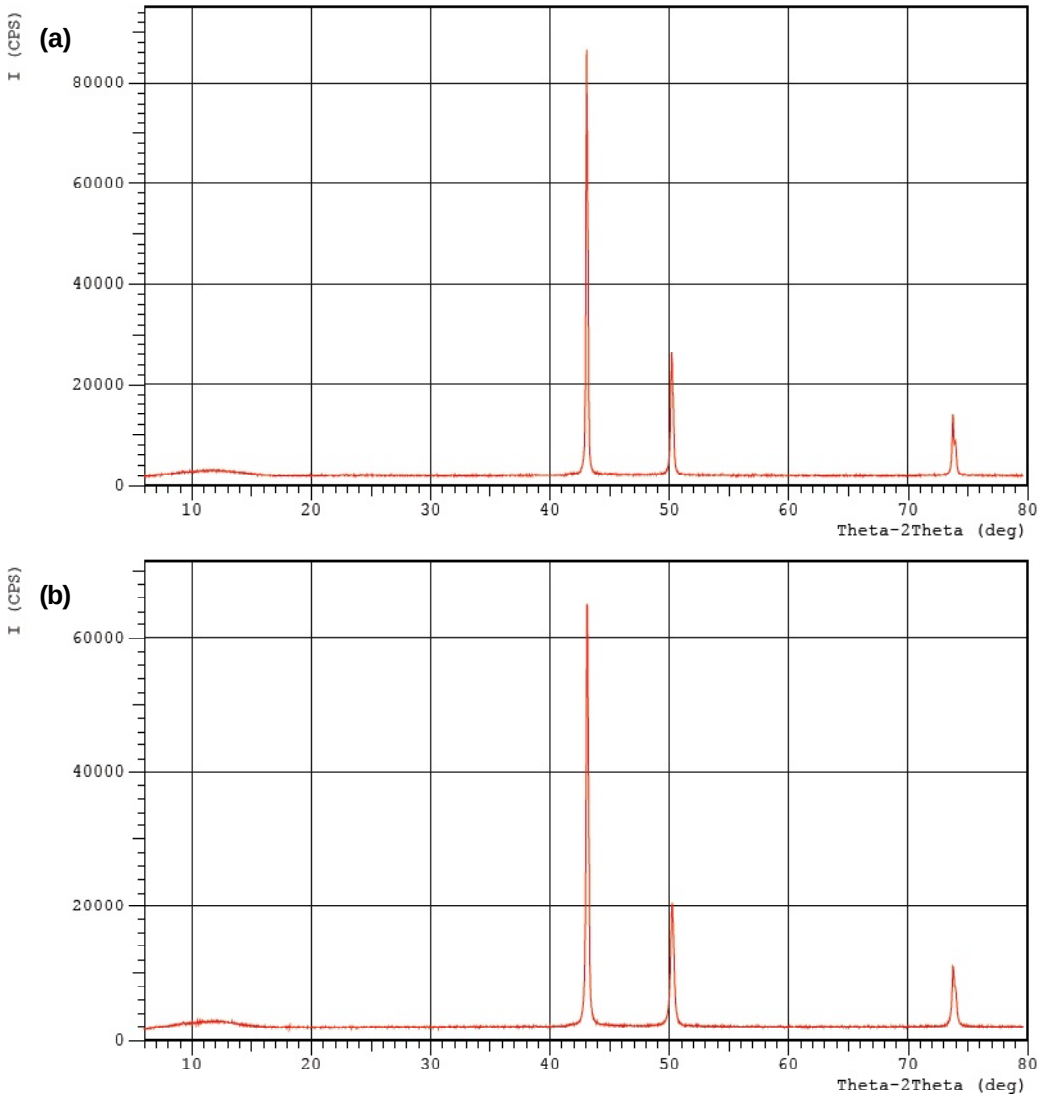

Fig. 1. XRD patterns of Sample 4: (a) outer surface, (b) inner surface.

the comparison of the results obtained for outer and inner Sample surfaces (Figs. 1a and 1b, respectively) demonstrated that the reflexes from XRD pattern corresponding to inner surface are slightly broadened as compared to the same peaks from outer surface pattern. This fact can be assumed as being due to smaller crystallite size typical for inner surface, i.e. for crystallites formed just at the film growth onset. The estimates of the linear dimensions typical for inner surface crystallites performed using Sherrer's formula are ~ 100-110 nm, while the same sizes estimated for outer size crystallites are ~180 nm. As will be shown below, this result agrees with the data obtained from SEM data.

SEM data were used to choose the optimal deposition conditions. As seen from Fig. 2 (Samples ##1-4, the general view of the surface, [32]), the effect of ethanol content in the electrolyte on the quality of the growing surface is evident. Indeed, Samples 1-3 were grown in the same electrodeposition cell. Sample 1 grown from the electrolyte without ethanol demonstrated rough and non-compact surface Fig. 2a. The excess of ethanol (Sample 2, 75 mL/L of ethanol, Fig. 2b) also resulted in rather rough sample surface, while the moderate addition (Sample 3, 37.5 mL/L of ethanol, Fig. 2c) showed acceptable results. Note that the use of the electrolyte with the latter ethanol content (Solution N3) in another cell geometry (Sample 4, Fig. 2d) also provided smooth and compact surface of the specimen. It should be also mentioned that in the similar cell geometry tests (Samples 1-3) Solution N3 electrolyte demonstrated the highest growth rate exceeding 300 μm per hour. So, the use of aqueous-ethanol electrolyte with a moderate (37.5 mL/L) content was considered as an optimal choice.

The comparison of the samples microstructure (see Fig. 3) gives an opportunity to choose the op-

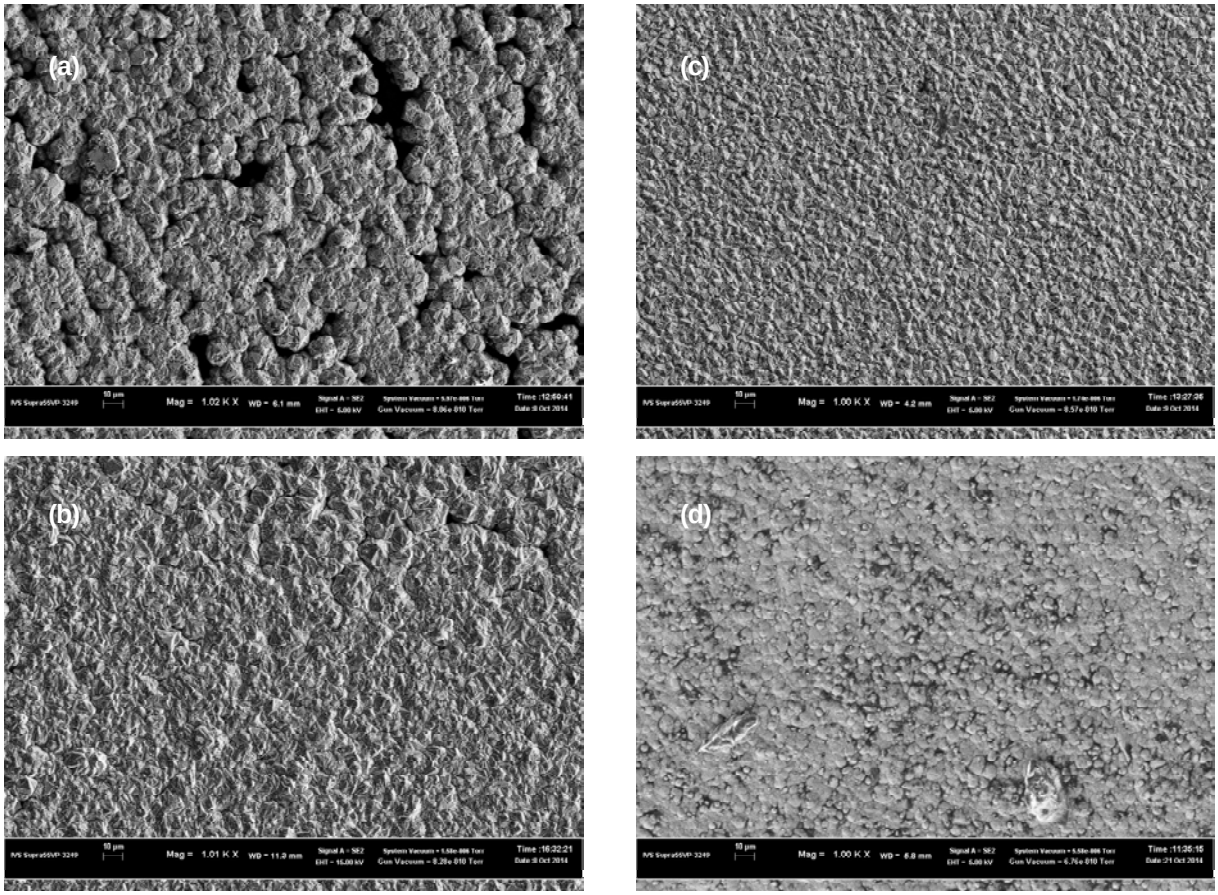

Fig. 2. SEM data for copper film surface: a,b,c,d – Samples 1,2,3,4, respectively.

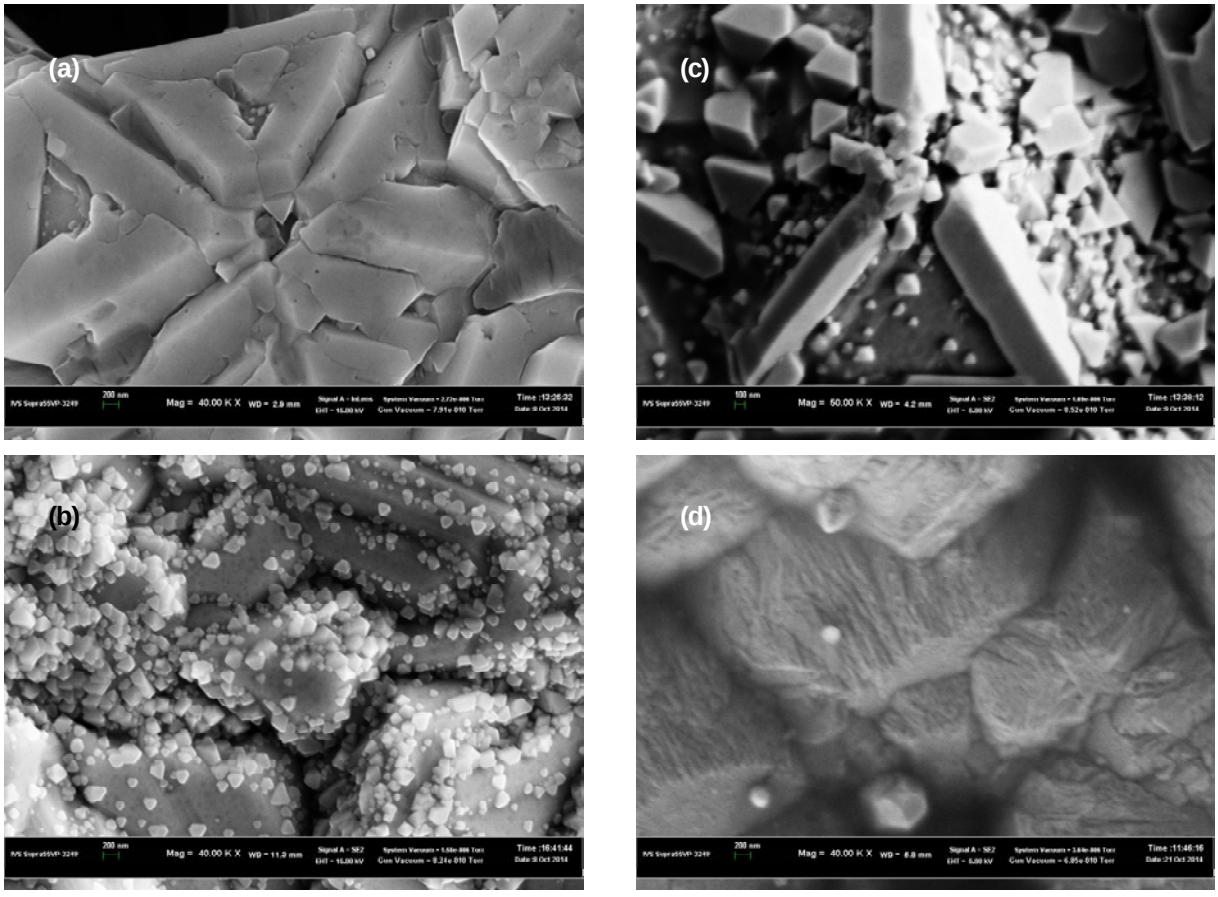

Fig. 3. SEM data for copper films microstructure: a,b,c,d – Samples 1,2,3,4, respectively.

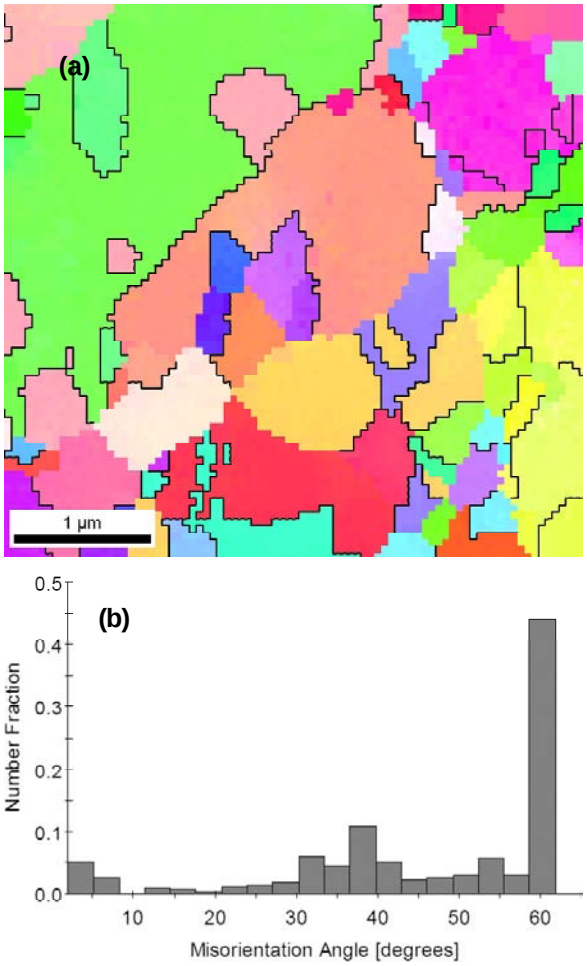

Fig. 4. EBSD data for electrodeposited copper (Sample 4): (b) typical IPF map of the sample surface; (b) misorientation distribution, peak at 60° corresponds to twin boundaries.

timal cell geometry. As seen from this figure, the use of cylindrical geometry with low anode-to-cathode ratio (Cell#1, Figs. 3a-3c) resulted in the random orientation: the grown film is neither epitaxial nor columnar, polycrystals oriented on the edges and planes of octahedrons or triangular prisms are observed here. On the contrary, the use of planar deposition cell geometry with high anode-to-cathode ratio (Cell#2, Sample 4) provided the uniform film growth, the additional experiments (see [32] for details) showed that the typical linear size of Sample 4 crystallites were nanoscaled, this result agree with the data estimated by XRD, similar conclusions were done from EBSD data.

EBSD results obtained for Sample 4 (see Fig. 4) indicated the presence of the significant amount of the twin boundaries. The typical example of the raw inverse pole figure (IPF) map acquired from Sample 4 surface without any polishing is shown in Fig. 4a, the black lines in this figure delineate twins.

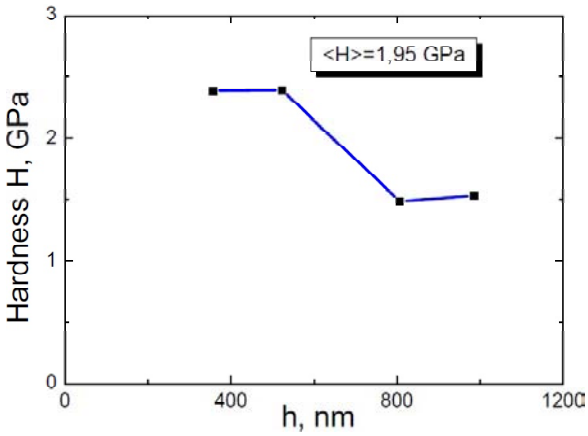

Fig. 5. Nanoindentation test results (a) The dependence of the average hardness values on the indentation depth; (b) The dependence of the average Young's modulus values on the indentation depth.

The fraction of twin boundaries here can be estimated as > 50%. Fig. 4b demonstrates the distribution of the grain boundary misorientation angles; note that the peak at 60° which corresponds to Σ3 boundaries. Total number fraction of twins estimated from this distribution is also more than 50 percent.

Summarizing the above results on Sample 4 microstructure, it can be concluded that this sample is nanostructured and possesses more than 50% of twin boundaries, thus, this sample can be treated as NT copper.

Nanoindentation tests were carried out for Sample 4 (5, 10, 15, and 20 mN maximal loadings; the diamond Berkovitch indenter; loading/unloading rate 0.5 mN/s). Hardness and elastic modulus were calculated using Oliver-Pharr approach, see, e.g. [33]. Fig. 5a demonstrates the dependence of average hardness values on the indentation depth, the average hardness value from these data was calculated as 2.4 GPa for the indentation depth less than 500 nm; it decreases down to 1.5 GPa (37%) at the indentation depth of 800 nm. Young's modulus as a function of indentation depth curves was calculated. It was shown that the increase in the nanoindentation depth gives rise to the decrease in the Young's modulus from 48 to 23 GPa. So, the Young's modulus value can be evaluated as 60 GPa. The average elastic modulus calculated from Hertz curve [33] was estimated as 102 GPa.

Comparing the nanoindentation data with the results obtained for NT copper by L. Lu, one can conclude that the data for Sample 4 agree well with the results shown for NT copper. As for data reported by Pavithra et al. [27] for pure annealed copper foils and copper-graphene composite foils, it can be

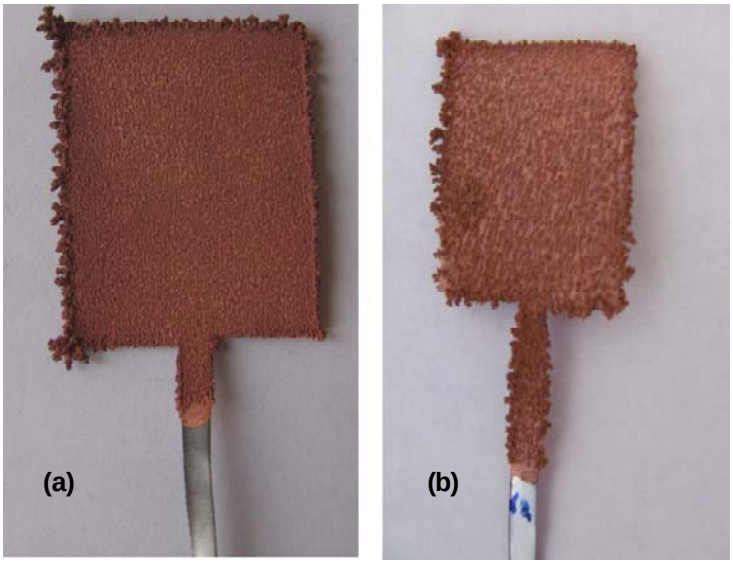

Fig. 6. Typical examples of copper-graphene foils produced at the preliminary step of the work: (a) sample synthesized at DC; (b) sample synthesized in a pulse regime.

stated that the results of the mechanical tests obtained for Sample 4 are ~ 2 times higher than those reported for the pure annealed copper and are close to the values determined for copper-graphene composite.

3. NANOTWINNED COPPER-GRAPHENE FOILS

Synthesis approach providing relatively simple pathway to produce NT Cu foils was discussed in the previous Section. This approach was applied to NT copper- graphene foils production. The procedures described for copper-carbon (graphene, nanotubes, nanowires, etc.) composites deposition in [23,24,27,34-38] were taken into account. The preliminary results of this work were reported in our paper [39].

Exfoliated graphite was chosen as a graphene source for the synthesis procedure. As it is known, see e.g. [40], micromechanical splitting is a very effective way to convert exfoliated graphite into graphene; such a splitting could by realized via high energy ball milling coupled with mechanical activation. Indeed, Raman spectroscopy of the synthesized samples (discussed below in this Section) proved the complete conversion of the exfoliate graphite into graphene for a number of samples. However, the usual result of such treatment was the formation of some graphene-graphite mixture with high graphene content. So, to prepare the graphene source for the electrolyte, the mixture of $CuSO_4*6H_2O$ with exfoliated graphite was produced, the graphite content here was 3 wt.%. This powder mixture was subjected to micromechanical splitting by ball milling coupled with mechanical activation. Pulversette 6 FRITSCH planetary ball mill was used for this task, splitting was performed in agate vessels with a set of agate balls at 400 rpm. A number of process durations were tested, as a result four hours treatment was chosen as providing the optimal graphite-to-graphene conversion level. XRD patterns (Shimadzu XRD-6000) of the initial $CuSO_4*6H_2O$ – exfoliated graphite mixture were compared with those obtained for the mixture subjected to micromechanical splitting. The peak broadening and the peak intensity decrease were observed in the patterns of the treated mixture. These facts could be considered as an indirect support of the graphite-to-graphene conversion [40]. The treated mixture was used to prepare the graphene electrolyte.

Electrochemical deposition was used for foils production, the main parameters of the process were based on the results of our previous work [32], see Section 2 above. In order to obtain electrolytes with 0.1, 0.2, and 0.4 g/L graphene content water-ethanol copper sulfate solution (Solution N3) was mixed with graphene suspension. The geometry of the electrochemical deposition cell was similar to that in case of Sample 4 (see Table 1 and Section 1 above), both DC and pulse regime deposition were used. The typical photos of the samples produced are presented in Fig. 6. Fig. 6a demonstrates the surface of the sample manufactured from the electrolyte with 0.2 g/L graphene content at 0.25 A DC applied for 2 hours. To ensure the uniformity of the suspension, graphene containing electrolyte was

treated by ultrasound (35 kHz for 15 min) prior the electrochemical experiment. As seen from the figure, the surface quality of this sample was insufficient: it is not smooth, the growth process resulted in randomly oriented polycrystals. In addition, the compactness of the coating was very low. In any case, the quality of the coating surface can not be compared with the smooth and compact surfaces obtained in [32] for pure nanotwinned copper. Note that similar results were obtained for electrolytes in the whole graphene content range. Some minor modifications of samples manufacturing procedure (cathode graphitization, additional electrolyte premixing, etc.) did not provide acceptable foil quality. Fig. 6b is a typical photo of the sample produced in the pulse regime. According [27], the use of pulse regime could improve the uniformity of graphene distribution in copper-graphene composites; the authors of [27] considered this fact as following from the specific features of the process kinetics. The sample shown in Fig. 6b was manufactured at 44 mA, 20 V peak intensity; the on- and off-times here were 0.02 and 2 s, respectively. As seen from the figure, the quality of samples produced in a pulse regime is very close to that in case of DC regime. Despite all potential benefits of pulse regime mentioned in [27], the increase in the deposition duration makes it application rather impossible for copper-graphene composites synthesis. Indeed, too long precipitation time results in graphene agglomeration and graphene containing suspension destabilization.

So, the preliminary work on NT Cu-Gr foils production identified two major problems briefly mentioned the Introduction Section.

(i) The problem of graphene content stabilization during the long-tem deposition. Indeed, the decrease in the deposition rate generally increases the quality of the films; this can be explained by the increase in the time granted to the deposited unit (ion, atom, molecule, etc.) to add to proper surface structural unit finding the optimal and preferable one. Hence, process duration should be increased up to 2-3 hours to get reasonable foil thickness. However, graphene agglomeration and graphene-containing additive precipitation occur during the deposition process resulting in the destabilization of Gr containing suspension. As a result, graphene distribution in the foil is fairly non-uniform. Moreover, possible precipitation of the agglomerated graphene flakes on the cathode surface additionally decreases the growing film quality.

(ii) The problem related to required nanotwins presence in the foil structure. The presence of graphene in the electrolyte gives rise to the additional growth centers appearance on the cathode surface at the very first stage of film formation. This results in the microstructure consisted of copper polycrystals with random orientation instead of nanosized twins produced under the same conditions without graphene.

In the recent works [41-43] novel approaches for nanotwinned copper-graphene composites were suggested. As it is well known, the addition of non-ionic surfactants could stabilize the concentration of additives powder in the solution for a long time. The requirements for such type of surfactants are evident: they should possess high solubility in the water, high molecular mass, and demonstrate the absence of micelles formation in the acid solutions. Following these requirements, commercially available non-ionic surfactants polyacrilic acid (PAC) and Pluronic F-127 (PLU) were chosen. These surfactants were added to the graphene suspension at the step of its preparation. Since there was a strict necessity to avoid contamination of the foil, the amount of surfactants was rather low: their content in the electrolyte varied from 25 to 100 ppm. The deposition process here was quite similar to described above, however, some features should be mentioned: (i) in addition to previously used exfoliated graphite, commercially available graphene-graphite mixture produced by low-temperature graphite splitting (Active-Nano Co., Russia) was used as a graphene source. The general idea of such substitution was to compare the results obtained with the graphene-graphite mixture produced following the developed procedure with those for the commercial one in order to evaluate the level of the resulting level of the graphite-to-graphene conversion. It was shown that the results for both graphene-graphite mixtures agree well, thus, it can be concluded that the micromechanical splitting approach used in our technology provides necessary level of the graphite-to-graphene conversion. (ii) PAC or PLU surfactants were added to the graphene suspension as mentioned above.

Fig. 7 demonstrates the typical photos of the samples produced in the deposition process with surfactants. As seen from the comparison of Figs. 6 and 7, the addition of surfactants (both PAC and PLU), significantly increases the quality of the growing film. Let us discuss the results reported in [41,42] in more detail. A number of samples were synthesized at this step of the work, they are listed in Table 2.

The first task of the experimental investigation was to prove the graphene incorporation into the foil matrix. Fig. 8 demonstrates XRD patterns obtained for Sample 9 (synthesized from the electrolyte con-

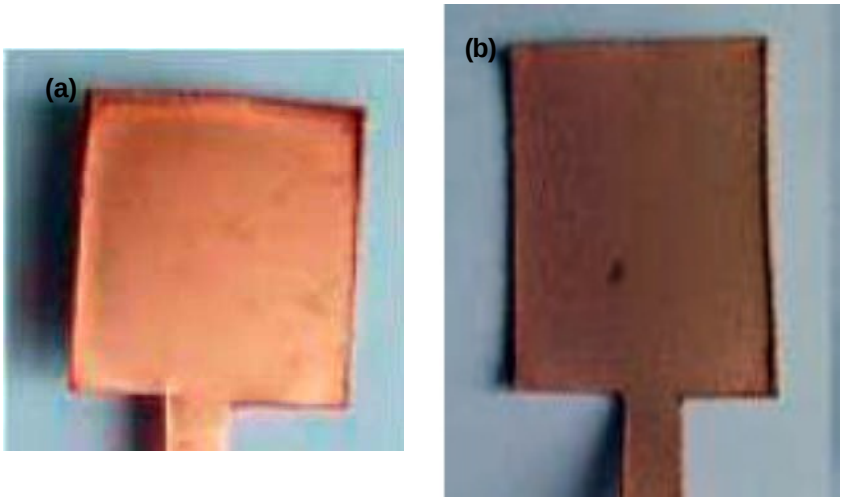

Fig. 7. Typical examples of copper-graphene foils produced from the electrolytes containing 25 ppm surfactants: (a) PAC; (b) PLU.

Table 2. List of the NT Cu-Gr samples.

Sample	Surfactant	Surfactant content in the electrolyte, ppm	Graphene content in the electrolyte, g/L
6	PAC	25	0.05
7	PAC	25	0.1
8	PAC	50	0.1
9	PAC	100	0.1
10	PLU	25	0.1
11	PLU	50	0.1

taining 0.1 g/L of Gr). As seen from the comparison of these patterns with those obtained for pure nanotwinned copper (see Fig. 1), the basic difference is in the appearance of the reflex at $2\theta=26°$; this reflex is attributed to carbon. Note that the sensitivity limit of XRD analysis is usually stated to be ~3-5 wt.%, hence, it was reasonable to assume that the level of the graphene incorporation in the foil matrix is rather high. The estimates of the crystallinity level (crystal-to-amorphous ratio) following from XRD data indicated the significant dependence of this level on surfactant content in the electrolyte. 48% and 82% levels were calculated for Samples 9 and 11, respectively; these values can be compared with the results obtained previously [32] for pure NT Cu: it was estimated as 69%. Thus, XRD study proved the significant graphene incorporation into the foil matrix, showed the high crystallinity level of the Samples, and demonstrated the possibility to control this level in a wide range via the optimization of surfactant content and its type.

SEM results were considered to understand the effect of surfactants addition on the foils microstructure. As an example, Fig. 9 compares SEM data for Samples 9 and 10 (with maximal and minimal surfactants content, 100 and 25 ppm, respectively). As seen from the figure, surfactant addition provides close to epitaxial film grows. The surfactant content affects the properties of the grown foil: higher amount of surfactant (Fig. 9a) results in more uniform surface; less amounts (Fig. 9b) gives rise to the formation of the evident crystal structure with sharp edges. The typical linear dimensions of the objects on the sample surface are relatively higher in case of higher surfactant content (Sample 9); these data correlate with the above discussed XRD results on samples crystallinity level. It could be assumed that the nature of surfactant also affects the foil microstructure: PAC addition results in some amorphization, while PLU increases sample crystallinity.

It is important to state that, in spite of the surfactant type, the foil quality is quite acceptable: no macrodefects were observed for most samples, the samples studied demonstrated relatively uniform surface with high integrity. Note that some samples deposited from the electrolytes with high graphene content and PAC concentrations were characterized by the presence of some pores with typical linear dimensions of 1 μm (see the example in Fig.

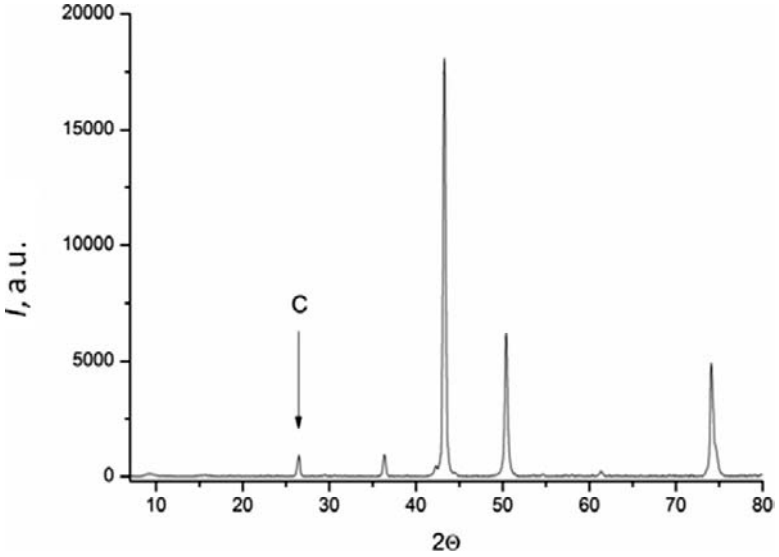

Fig. 8. XRD patterns of Sample 9.

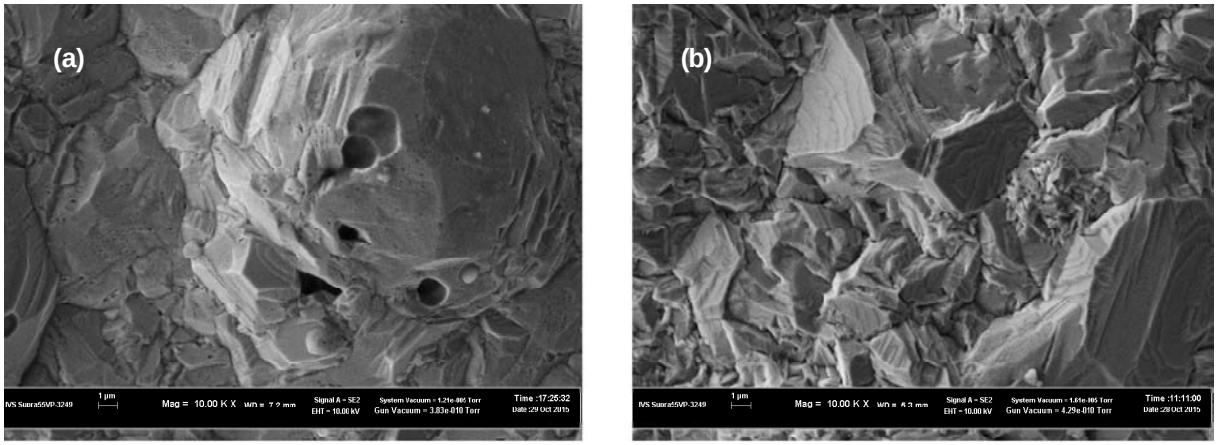

Fig. 9. SEM data for Samples 9 and 10, figures (a) and (b), respectively.

9a, dark circles). Since such pores are typical for samples deposited at high graphene content in the electrolyte, it is reasonable to suggest that their formation is due to the presence of relatively large graphene inclusions (agglomerates?) on the growth surface. Thus, the results of SEM investigations demonstrated that even a small addition of non-ionic surfactants gives an opportunity to effectively stabilize graphene containing suspensions and, as a result, to produce uniform foils characterized by the smooth surface. The possibility to control the NT Cu-Gr foils microstructure via the variation of the surfactants-to-graphene ratio in the electrolyte was shown.

EBSD investigations were carried out to clarify the nature of samples synthesized, distributions of the misorientation angles and grain sizes are presented in Figs 10 and 11. The obtained data on misorientation angles can be compared with the results detected for pure NT Cu, see Fig. 4b. It was stated above that the fraction of misorientation angles equal to 60° (twinned boundary type indication) in case of pure NT copper was ~ 50%. As seen from Fig. 10, the use of PLU surfactant (Figs. 10e and 10f) resulted in a similar distribution; in can be assumed that the fraction in the 60° angle boundaries increases with the increase in PLU content. The effect of PAC surfactant is more complicated (see Figs. 10a-10d). Generally, the increase in the amorphization level and higher graphene content appears to be typical for the use of PAC surfactant (see the discussion of XRD and SEM results above) resulted in some decrease in fraction in the 60° misorientation angles, sometimes down to 40% or even less. The optimal graphene/surfactant ratio in case PAC as a surfactant was established (see Fig. 10b); the use of such an optimal combination results in the misorientation angles distribution similar to that detected for pure NT copper.

Comparing the results of grain size determination (Fig. 11), one can conclude the following. Generally, all samples synthesized are characterized by the grain size in the range 0.5-10 μm. However, one can control the grain size distribution in the foil

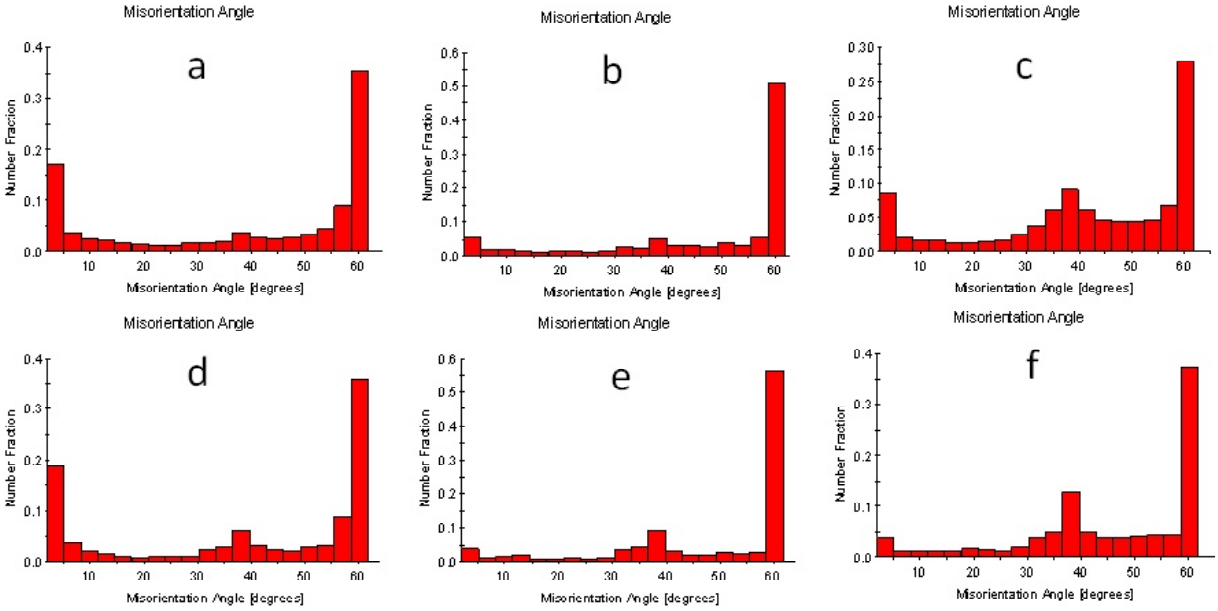

Fig. 10. Misorientation angle distributions from EBSD data: (a)-(f) – Samples 6-11, respectively.

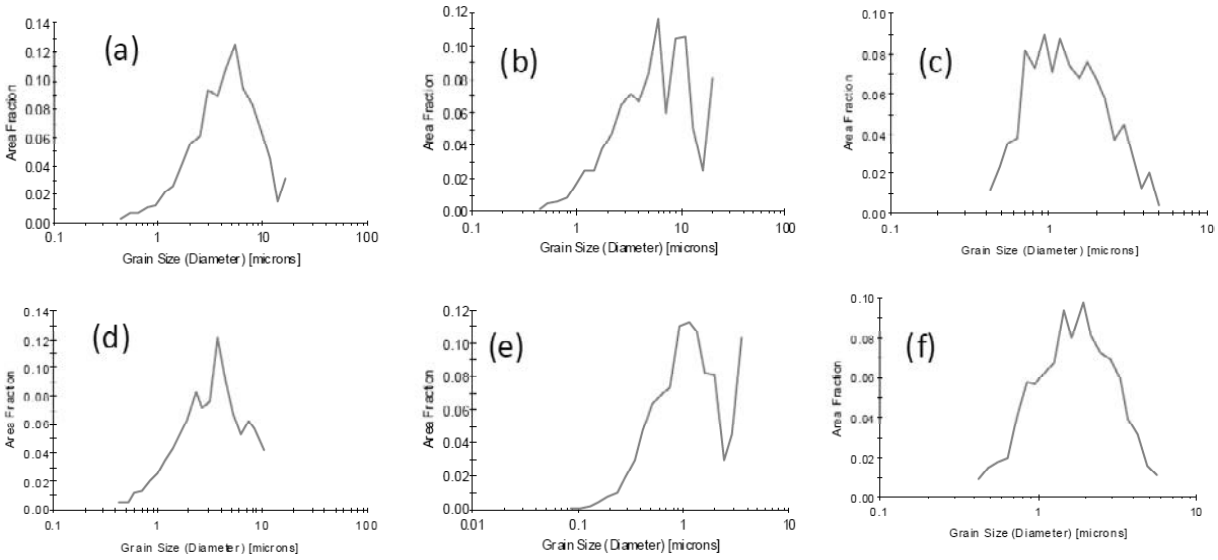

Fig. 11. Grain size distributions from EBSD data: for Samples 6-11, images (a)-(f), respectively.

varying the synthesis conditions. Indeed, lower ranges of the grain size were shown for Samples 8 and 10 (maximum at ~ 1-1.5 μm), while Samples 6,9, and 11 contained larger grains (distribution maximum at ~ 5-7 μm). The distribution maximum in case of the above discussed Sample 7 (PLU surfactant, sample with misorientation angle distribution similar to that for pure NT copper, see Fig. 10b) was shifted to 8-10 μm region; in addition, some part of grains had sizes exceeding 10 μm.

Thus, EBSD study confirms the nanotwinned nature of the grown film. In addition, the possibility to vary the foils microstructure by proper electrochemical deposition procedure choice was demonstrated.

Transmission electron microscopy analysis (TEM, Jeol JEM-1230) was carried out to obtain the evident support for the above assumptions, see Figs. 12 and 13. Fig. 12 demonstrates typical nanotwinned structures proving the conclusion that graphene and surfactant added in the electrolyte along with graphene introduction into the foil matrix did not generally disturb NT copper mode, this fact agrees with above discussed EBSD data. Fig. 13 shows the graphene inclusions in the foil (extended dark objects on TEM images, see more details in [24] and our previous work on Al-Gr composites [44)].

Another approach to improve the nanotwinned modification of the material was the following [43,45]. Thin buffer layer (0.1-0.15 μm) of pure NT Cu was

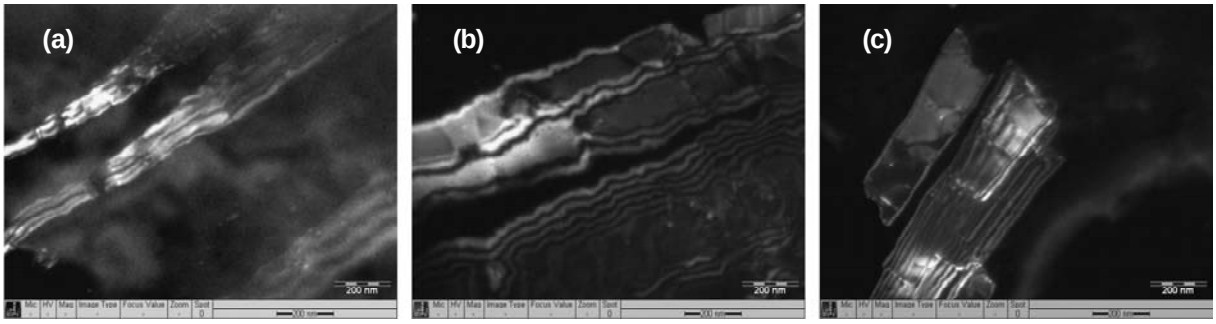

Fig. 12. TEM data demonstrating structures typical for nanotwinned copper: (a) Sample 8, (b) Sample 9, (c) Sample 10.

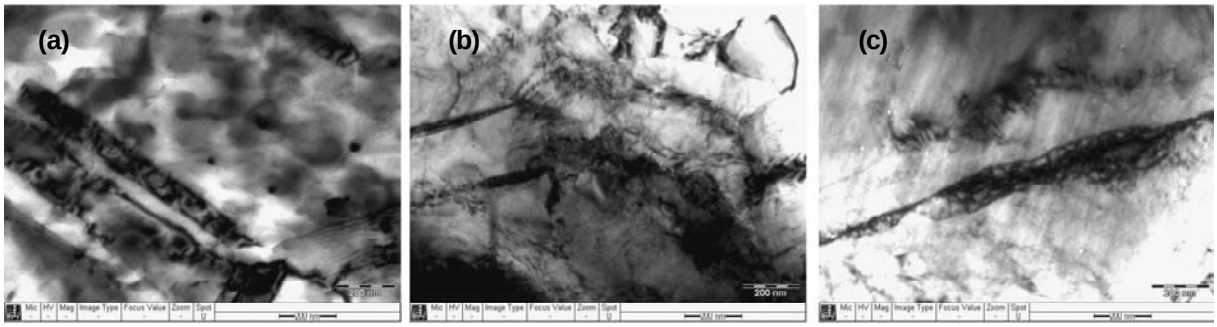

Fig. 13. TEM data demonstrating structures typical for graphene inclusions: (a) Sample 7, (b) Sample 8, (c) Sample 10.

deposited on the cathode surface. In doing so, the additional graphene precipitates/agglomerates working as the additional growth centers on the cathode surface were eliminated at the very first step of the deposition. This approach provided the deposition of the pure NT Cu and inheritance of this nanotwinned nature by the foil metal bulk during the following deposition from the Gr-containing electrolyte. So, graphene-free electrolyte (see Section 2) was used at the first step of the deposition (0.25 A for 30 min) and graphene/surfactants containing electrolyte (see current Section) was used to deposit the main part of the foil (0.25 A for 120 min). Table 3 lists the composition of the Samples synthesized following bi-layered technique.

The analysis of XRD and SEM study performed for these bi-layered samples indicated that the preliminary grown pure NT layer did not significantly affect neither phase composition of the foil (carbon additions were detected by XRD) nor its microstructure. Indeed, the surface of the inner layer (NT Cu layer adjacent to the cathode) according to SEM data was close to that of pure NT copper (See Section 2), while the outer surface of the film (NT Cu – Gr) correlated with the data obtained for similar foil produced by one-layer technique.

Table 3. List of Samples synthesized following bi-layered technique.

Surfactant	Sample	Graphene content, g/L	Surfactant content, ppm
PLU(Pluronic–F-127)	12	0.05	25
	13	0.1	25
	14	0.1	50
	15	0.25	50
	16	0.25	100
	17	0.5	50
	18	0.5	100
PAC(Polyacrilic acid)	19	0.05	25
	20	0.1	25
	21	0.1	50
	22	0.1	100

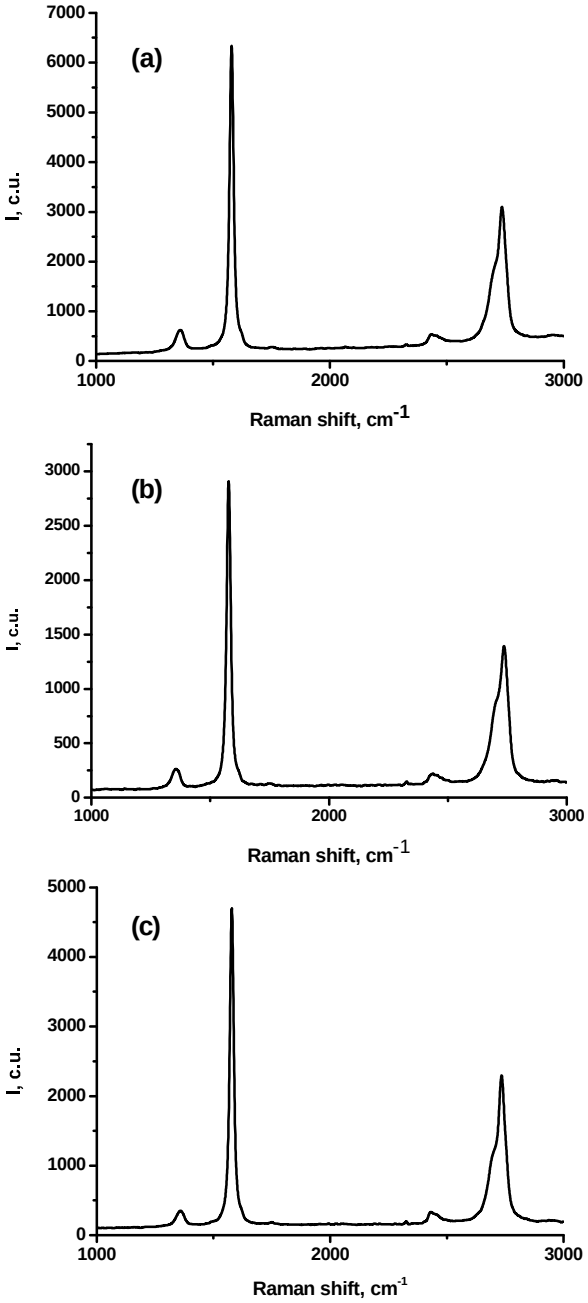

Fig. 14. Raman spectra of NT Cu-Gr bi-layered foils, Samples15 (a), 16 (b), and 18 (c).

Raman spectroscopy (SENTERRA, T64000, excitation wave length 488 nm, gate voltage 40 V) was used to identify carbon allotropes in the deposited samples. Fig. 14 presents some results for the samples deposited using PLU surfactant, samples produced from electrolyte with PAC surfactant demonstrated similar results (for more details see our works [43,45]). The ratio between the intensities of G and 2D peaks (1550 and 2880 cm^{-1}, respectively) indicated that graphene in the foils presented as few-layered flakes; a number of layers in the flake can be estimated as 4-6 [46]. The comparison of the Raman spectra obtained for the foils deposited from PLU-containing electrolyte indicated that the relative number of mono- and bi-layered graphene flakes in the resulting foils is higher during the deposition from more concentrated graphene containing suspensions and increased surfactant content. The comparison of peaks intensity showed that the maximal graphene incorporation was obtained for Samples 13, 15, and 18. Hence the optimal ratio for graphene incorporation in case of PLU surfactant was determined as 0.1 g/L graphene and 25 ppm PLU. For PAC surfactant, the maximal graphene incorporation was shown for Sample 21, the optimal ratio here was 0.1 g/L graphene and 100 ppm PLU.

The obtained results give us the possibility to clarify the mechanisms of NT copper-graphene foils formation in the presence of surfactants. Let us discuss them in some more detail. SEM data demonstrated high integrity and uniformity of the foil surfaces deposited from the PLU-containing electrolyte. The deposition of the thin buffer layer of NT Cu provides the elimination of the difference between the lattice parameters of iron (the main component of the cathode material) and copper, 2.866 and 3.615 Å, respectively. The absence of large-size incorporations in the metal matrix of the foil proves the positive effect of surfactant: the elimination of graphene (graphite) agglomeration during the foil deposition.

The following effect of the electrolyte composition (graphene-to surfactant ratio) could be revealed on the microstructure of Cu-Gr foils. The resulting foil is quite uniform and its surface possesses low roughness in case of electrolytes with relatively low Gr and surfactants contents. Since PLU (as well as PAC) is a non-ionic surfactants, its addition increases the suspension viscosity providing the graphene stabilization in the electrolyte. In turn, this stabilization decreases the deposition rate and induces to the appearance of a large number of the growth centers; these centers are properly distributed on the growing surface providing the simultaneous and uniform growth of the copper polycrystals. The increase in the Gr content at a given surfactant amount results in some stabilization decrease due to the lack of the surfactant; as a result, relatively large copper crystals are observed as inclusions in the uniform foil matrix. The formation of these large crystals is stopped at the surfactant content increase (up to 50 ppm), however, the integrity of the deposited foil becomes low. The attempt of simultaneous increase in the graphene content increases the deposition rate resulting in some fine-grained

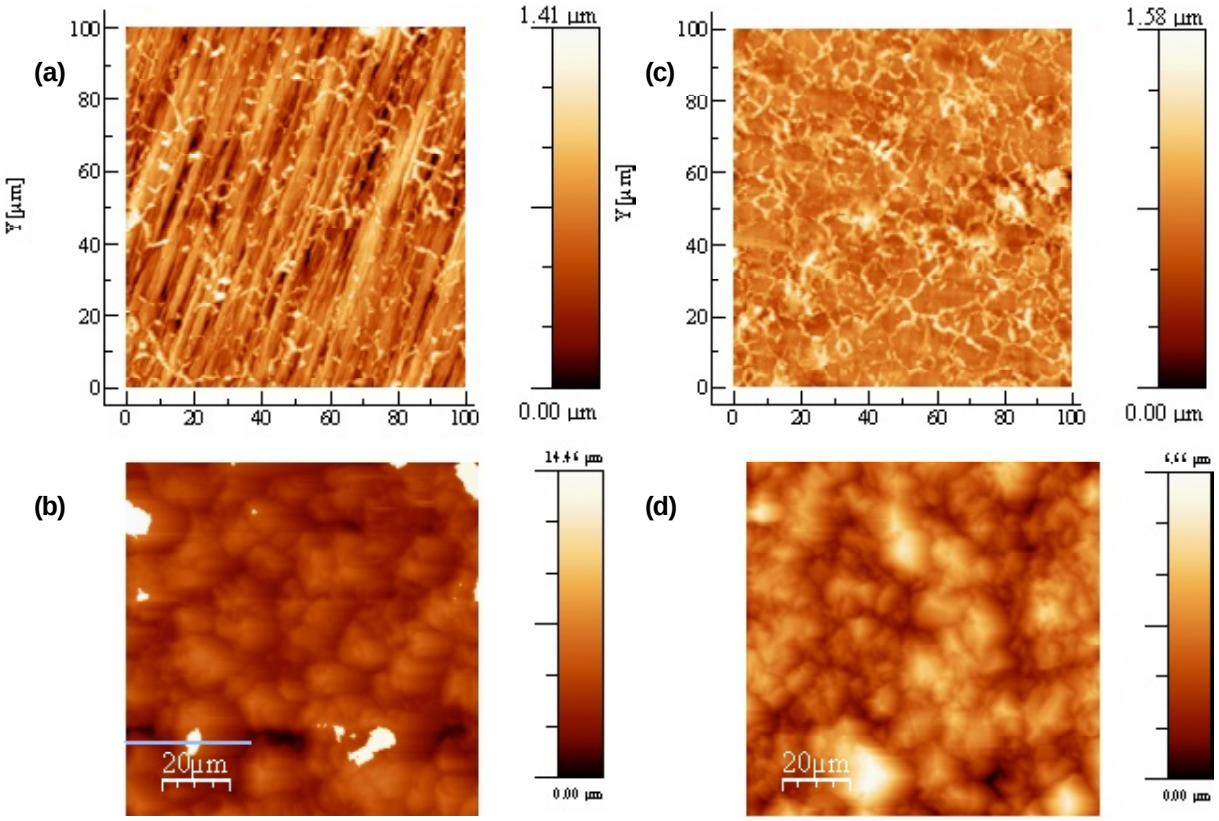

Fig. 15. AFM results for the foils produced from: (a) and (b) – PLU-containing electrolyte, 25 and 50 ppm, respectively; (c) and (d) PAC-containing electrolyte, 25 and 50 ppm, respectively.

structure formation. This structure consists of hexagonal copper crystals with the typical linear dimension of 0.5-10 μm.

In case of PAC incorporation as suspension stabilizer, the bi-layer technique also increases the quality of the deposited foil. Indeed, the microstructure of the produced samples was more uniform than that in case of the one-step copper-graphene deposition. However, this structure is more rough as compared with that manufactured from PLU-containing electrolyte at the same graphene-to-surfactant ratio. Some microdefects as well as contaminations (residual PAC molecules or their fragments) were observed at the foil surface. The increase in the surfactant contents in this case leads to cavities and pores formation.

The above discussion can be illustrated by atomic force microscopy (AFM, EasyScan (Nanosurf), 100 μm^2 region was scanned with 390 nm resolution for 2 s). Fig. 15 compares the AFM images obtained for the foils produced from PLU- and PAC-containing electrolytes (a, b and c,d, respectively). As seen from Figs. 15a and 15b, the increase in PLU surfactant contents from relatively low one (25 ppm) up to a higher content (50 ppm) evidently changes the deposition mechanism. Obviously, low PLU concentration is enough to stabilize the suspension and the foil surface is quite uniform. However, some preferable crystal growth direction is observed for processes with higher surfactant concentration. Foils produced using PAC-containing electrolyte (Figs. 15c and 15d, 25 and 50 ppm, respectively) are characterized by rather rough structure containing large-size objects. The increase in PAC content results in the increase of sample non-uniformity: according to the estimates

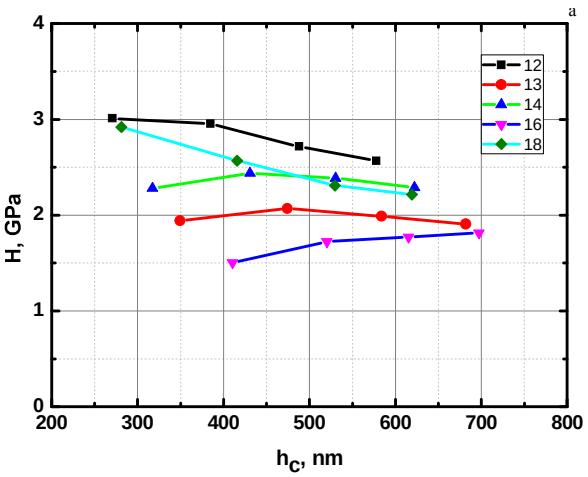

Fig. 16. Microhardness values for the inner surface of the foils manufactured from the PLU-containing electrolytes.

from AFM data, the surface roughness increases nearly twice with the increase in PAC content from 25 to 100 ppm.

The microhardness of the foils was detected by nanoindentation, see our work [45] for more details. It was stated that the microhardness of the outer surface of the foils was quite similar to the results reported for pure NT copper (see Section 1). However, the inner surface of the foil (surface adjacent to the cathode) that is the bi-layer combination of pure NT Cu with NT Cu-graphene layer demonstrated the unique microhardness of ~ 3 GPa, see Fig. 16. Note that the results presented in these figures deals with foils produced from PLU-containing electrolyte, the results for less uniform and more rough foils manufactured from PAC-containing electrolyte were lower. In agreement to SEM and AFM data, the best results were obtained for foils with low graphene/ surfactant contents in the electrolyte.

4. CONCLUDING REMARCS

This review summarizes the work on nanotwinned copper – graphene foils synthesis. It was shown that the use of bi-layered technique gives the opportunity to increase the quality of the foils. The technique is based on the thin buffer layer of a pure nanotwinned copper deposition at the first step of the foil production. The absence of the additional growth centers determined by the presence of graphene in the electrolyte provides the possibility to grow copper in its nanotwinned mode. This nanotwinned modification is further inherited by the metal matrix of the foil deposited at the second step of the process; graphene-containing electrolyte is used at this step. The use of surfactants gives an opportunity to stabilize graphene concentration in the electrolyte during long0term deposition. Pluronic-F127 and Polyacrilic acid were tested as non-ionic surfactants; the changes in the basic deposition mechanisms were discussed regarding to graphene-to-surfactant ratio in the electrolyte. It was shown, that the use of Pluronic-F127 is more preferable, the optimal process conditions providing the production of bi-layered nanotwinned copper – graphene foils with unique microhardness (up to 3 GPa) were suggested.

ACKNOWLEDGEMENTS

The work was supported by the Ministry of Education and Science of Russian Federation (Zadanie № 16.3483.2017/ПЧ). Authors are grateful to the Center for Optical and Laser Materials Research of St. Petersburg State University for Raman spectroscopy data.

REFERENCES

[1] I.A. Ovid'ko and A.G. Sheinerman // *Rev. Adv. Mater. Sci.* **44** (2016) 1.
[2] Y. Morris Wang, Frederic Sansoz, Thomas La Grange, Ryan T. Ott, Jaime Marian, Troy W. Barbee Jr and Alex V. Hamza // *Nature Materials* **12** (2013) 697.
[3] T. A. Furnish and A. M. Hodge // *Apl. Mater.* **2** (2014) 046112-1.
[4] I.J. Beyerlein, X. Zhang and A. Misra // *Annu. Rev. Mater. Res.* **44** (2014) 329.
[5] Lei Lu, Yongfeng Shen, Xianhua Chen, Lihua Qian and K. Lu // *Science* **304** (2004) 422.
[6] L. Lu, X. Chen, X. Huang and K. Lu // *Science* **323** (2009) 607.
[7] Z.S. You, L. Lu and K. Lu // *Scripta Materialia* **62** (2010) 415.
[8] Z.S. You, L. Lu and K. Lu // *Acta Materialia* **59** (2011) 6927**.**
[9] Zesheng You, Xiaoyan Li, Liangjin Gui, Qiuhong Lu, Ting Zhu, Huajian Gao and Lei Lu // *Acta Materialia* **61** (2013) 217.
[10] In-Chul Choi, Yong-Jae Kim, Y. Morris Wang, Upadrasta Ramamurty and Jae-il Jang // *Acta Materialia* **61** (2013) 7313**.**
[11] C. Lee, X. Wei, J.W. Kysar and J. Hone // *Science* **321** (2008) 385.
[12] J. Wang, Z. Li, G. Fan, H. Pang, Z. Chen and D. Zhang // *ScriptaMaterialia* **66** (2012) 594.
[13] Z. Li, G.L. Fan, Z.Q. Tan, Q. Guo, D.B. Xiong, Y.S. Su, Z.Q. Li and D. Zhang // *Nanotechnology* **25** (2014) art. 325601.
[14] A. Upadhyaya and G.S. Upadhyaya //*Mater. Des*. **16** (1995) 41.
[15] A. Chrysanthou and G. Erbaccio // *J. Mater. Sci*. **30** (1995) 6339.
[16] B.M. Girish, Basawaraj, B.M. Satish and P.K. Jain // *J. Mat.: Des. Appl*. **226** (2012) 316.
[17] S. Islak, D. Kyr and S. Buytoz ***//*** *Science of Sintering* **46** (2014) 15.
[18] Y.H. Hu, O.A. Shenderova, Z. Hu, C.W. Padgett and D. W. Brenner // *Rep. Prog. Phys.* (2006) 1847.
[19] G. Chai, Y. Sun, J. J. Sun and Q. Chen // *J. Micromech.Microeng.* **18** (2008) 035013.
[20] W. M. Daoush and B. K. Lim // *Mater. Sci. Eng. A* **513-514** (2009) 247.
[21] M.E.Mendoza and I.G.Solorzano// *Mater. Sci. Eng. A* **544** (2012) 21.

[22] K. Novoselov, A. Geim, S. Morozov, D. Jiang, Y. Zhang, S. Dubonos, I. Grigorieva and A. Firsov // *Science* **306** (2004) 666.
[23] K. Jagannadham // *Metallurgical and Materials Transactions B* **43B** (2012) 316.
[24] Y. Kim, J. Lee, M.S. Yeom, J.W. Shin, H. Kim, Y. Cui, J.W. Kysar, J. Hone, Y. Jung, S. Jeon and S.M. Yan // *Nature Communications* **4** (2013) 2114.
[25] Y.F. Shen, L. Lu, Q.H. Lu, Z.H. Jin and K. Lu // *Scripta Materialia* **52** (2005) 989.
[26] X. Zhang, A. Misra, H. Wang, T.D. Shen, M. Nastasi and T.E. Mitchell // *Acta Materialia* **52** (2004) 995.
[27] C.L. Pavithra, B.V. Sarada, K.V. Rajulapati, T.N. Rao and G. Sundararajan // *Scientific Reports* **4** (2014) 4049.
[29] *Nano twin crystal copper material with ultrahigh strength and superhigh conductivity as well as preparation method*, patent CN 1234914 C (2006).
[30] Da Kuang, L. Xua, L. Liua, W. Hua and Y.Wua // *Applied Surface Science* **273** (2013) 484.
[31] *Method for preparing nano-copper/graphene composite particles under assistance of ultrasonic wave*, patent CN 103769602 A (2014).
[32] V.G. Konakov, I.A. Ovid'ko, N.V. Borisova, E.N. Solovyeva, S.N. Golubev, O.Yu. Kurapova, N.N. Novik and I.Yu. Archakov // *Reviews on Advanced Materials Science* **39** (2014) 41.
[33] A.C. Fischer-Cripps, *Nanoindentation* (N.Y., Springer, 2004).
[34] J. Hwang, T. Yoon, S.Y. Jin, J. Lee, T.-S. Kim,S.H. Hong and S. Jeon // *Adv. Mater.* **25** (2013) 6724.
[35] T. S. Koltsova, L. I. Nasibulina, I. V. Anoshkin, V. V. Mishin, E. I. Kauppinen, O. V. Tolochko and A. G. Nasibulin // *J. Mater. Sci. Eng. B* **2** (2012) 240.
[36] K. Jagannadham // *J. Vac. Sci. Technol. B* **30** (2012) 03D109.
[37] C.T.J. Low, R.G.A. Wills and F.C. Walsh // *Surf. Coat. Technol.* **201** (2006) 371.
[38] Ch.Subramaniam, T. Yamada, K. Kobashi, A. Sekiguchi, D. N. Futaba, M. Yumura and K. Hata // *Nature Communications* **4** (2013) 2202.
[39] V.G. Konakov, O.Yu. Kurapova, N.N. Novik, A.S. Graschenko, A.V. Osipov and I.Yu. Archakov // *Materials Physics and Mechanics* **24** (2015) 61.
[40] L. Kvetkova, A. Duszova, P. Hvizdoš, P. Kun and C. Balázsi // *Scripta Materals*. **66** (2012) 793.
[41] V.G. Konakov, O.Yu. Kurapova, N.N. Novik and S.N. Golubev // *Materials Physics and Mechanics* **24** (2015) 382
[42] V.G. Konakov, O.Yu. Kurapova, N.N. Novik, S.N. Golubev,A.P. Zhilyaev, S.N. Sergeev, I.Yu. Archakov and I.A. Ovid'ko // *Rev. Adv. Mater. Sci.* **45** (2016) 1.
[43] O.Yu. Kurapov, V.G. Konakov, A.S. Grashchenko, N.N. Novik, S.N. Golubev and I.A. Ovid'ko // *Rev. Adv. Mater. Sci.* **48** (2016) 71.
[44] V.G. Konakov, I.A. Ovid'ko, N.V. Borisova, E.N. Solovyeva, S.N. Golubev, O.Yu. Kurapova, N.N. Novik and I.Yu. Archakov // *Rev.Adv. Mater. Sci.* **39** (2014) 41.
[45] O.Yu. Kurapova, V.G. Konakov, A.S. Grashchenko, N.N. Novik, S.N. Golubev, A.V. Orlov and I.A. Ovid'ko // *Materials Physics and Mechanics* **32** (2017) 58.
[46] V. Shakalova and A.B. Kaiser // *Woodhead publishing series in electronic and optical materials* **57** (2014) 401.